An efficient cobalt-nickel phosphate positive electrode for high-performance hybrid microsupercapacitors

Min Li, Chen Jia, Danyu Zhang, Yunyun Luo, Yintao Ma, Guoxi Luo, Libo Zhao, Lu Wang, Zhikang Li, Qijing Lin, et al.

An Efficient Cobalt-Nickel Phosphate Positive Electrode for High-performance Hybrid Microsupercapacitors

Min Li[a, b, c], Chen Jia[a, b], Danyu Zhang[a, b], Yunyun Luo[a, b], Yintao Ma[a, b], Guoxi Luo[a, b, c]*, Libo Zhao[a, b, c]*, Lu Wang[a, b, c]*, Zhikang Li[a, b, c], Qijing Lin[a, b, c], Ping Yang[a, b, c], Nan Zhu[a, b], Rabah Boukherroub[d], Zhuangde Jiang[a, b, c]

[a] *State Key Laboratory for Manufacturing Systems Engineering, International Joint Laboratory for Micro/Nano Manufacturing and Measurement Technologies, Xi'an Jiaotong University (Yantai) Research Institute for Intelligent Sensing Technology and System, Xi'an Jiaotong University, Xi'an 710049, China*

[b] *School of Mechanical Engineering, Xi'an Jiaotong University, Xi'an, 710049, China*

[c] *Shandong Laboratory of Yantai Advanced Materials and Green Manufacturing, Yantai 265503, China*

[d] *Univ. Lille, CNRS, Centrale Lille, Univ. Polytechnique Hauts-de-France, UMR 8520 - IEMN, F-59000 Lille, France*

*To whom correspondence should be addressed: Guoxi Luo (luoguoxi@mail.xjtu.edu.cn), Libo, Zhao (libozhao@mail.xjtu.edu.cn), Lu Wang (wang.lu@xjtu.edu.cn).

ABSTRACT

Flexible energy storage devices play significant role in wearable and portable electronics. Herein, a cobalt-nickel phosphate ($CoNiP_2O_7$) composite was synthesized on conductive carbon nanotubes (CNTs) substrate by facile one-step electrochemical deposition method, forming a binder-free $CoNiP_2O_7$@CNTs positive electrode for microsupercapacitors (MSCs). Combined with a CNTs substrate on the opposite side of interdigitated electrode, a $CoNiP_2O_7$@CNTs//CNTs hybrid MSC device was assembled. It displayed good electrochemical performance with a largest areal capacitance of 20.9 $mF \cdot cm^{-2}$ at 0.08 $mA \cdot cm^{-2}$ and an energy density of 2.9 $\mu Wh \cdot cm^{-2}$. To construct a self-powered solar cell energy storage system, the proposed MSC device was utilized for energy storage and further provided power for red light-emitting diode (LED), forming natural energy collection-conversion-storage-utilization system. The results of this study offer a simple design route for flexible energy storage devices.

***Keywords**: Microsupercapacitor; Cobalt nickel phosphate; Carbon nanotubes; Flexible; Energy storage system*

INTRODUCTION

With the development tendency of portable electronic products, microrobots and implantable devices, the demand for flexible micro-energy supply devices with high performance has grown significantly [1-3]. Microsupercapacitors (MSCs), as energy storage devices, hold promising application potential and generated tremendous attention, owing to their miniature size, safety, long lifespan, high power density, etc [4-9]. With the construction concept of natural energy collection-conversion-storage-utilization system, it is imminent to explore high-performance MSCs to make full use of natural resources. Like for any energy device, the electrode material and electrolyte play significant roles in enhancing the electrochemical performance.

From electrode materials aspect, battery-like and pseudocapacitive electrodes have been widely investigated, and the former exhibit larger capacitance ascribed to the fast surface redox reactions [10-16]. Typically, transition metal oxides/hydroxides/sulfides/phosphides/phosphates, such as Co_3O_4 [17], $Mn(OH)_2$ [18], MoS_2 [19], NiFeP [20], $NiCo(HPO_4)\cdot 3H_2O$ [21], etc. are prepared and applied as the positive electrodes in MSC device assembly. Owing to their open framework with numerous active sites, transition metal phosphates have been extensively researched among battery-like electrodes, evoking their application in supercapacitors (SCs) [22, 23]. However, reports on the application of transition metal phosphates as positive electrodes in MSC devices are scarce. Therefore, their application potential in MSCs deserves attention to explore the possibility to improve the electrochemical performance of the hybrid MSC devices. It will be an important attempt, and exploration of transition metal phosphates in MSCs application~~, which~~ is meaningful and significant.

In this work, $CoNiP_2O_7$ composite was synthesized by one-step electrochemical deposition method and further applied as a positive electrode in hybrid MSC device assembly. The interdigitated carbon nanotubes (CNTs) electrodes~~,~~ investigated in this study, owing to their ~~advantages of~~ good conductivity and 1D nanostructure~~s~~, were prepared using the spraying-coating technique. One side of the interdigitated CNTs was utilized as the negative electrode directly, and the other side acted as the conductive

substrate for $CoNiP_2O_7$ deposition, forming $CoNiP_2O_7$@CNTs//CNTs hybrid MSC device. The assembled MSC exhibited the largest areal capacitance of 20.9 $mF \cdot cm^{-2}$ at 0.08 $mA \cdot cm^{-2}$ and favorable rate performance of 67% compared with the value measured at 0.5·$mA \cdot cm^{-2}$. The corresponding energy and power densities of the MSC device were respectively 2.9 $\mu Wh \cdot cm^{-2}$ and 41.3 $\mu W \cdot cm^{-2}$. Moreover, the MSC was applied to store the energy collected by solar cells in the natural energy collection-conversion-storage-utilization system, which could normally work and supply a red light-emitting diode (LED), indicating promising application potential as a flexible micro-energy storage device.

EXPERIMENTAL SECTION

Fabrication of the interdigitated CNTs symmetric electrodes. To construct a conductive substrate for further synthesis of $CoNiP_2O_7$ composite, 1D CNTs with good conductivity were chosen as the candidate. In the first step, a homogeneous dispersion of 135 mg of CNTs in 135 mL of ethanol was prepared under ultrasonication for 1 h. Then, the polyvinyl chloride (PVC) substrate was coated with a ~~Tungsten~~ tungsten mask, along with interdigitated shapes fabricated by laser processing method. In the following step, the CNTs dispersion was sprayed onto the flexible PVC substrate, forming the interdigitated symmetric electrodes. The width of one tooth was set as 1 mm, and the spacing distance was ~~fabricated as~~ 500 μm.

Preparation of $CoNiP_2O_7$ electrode. To build a hybrid MSC, one side of the CNTs symmetric electrodes acted as the working electrode (WE) and Pt plate ~~worked~~ was used as the counter electrode for electrodeposition of $CoNiP_2O_7$ composite. As illustrated in the schematic fabrication process depicted in **Fig. S1**, the electrodeposition process was conducted in an aqueous solution (100 mL) consisting of 290.8 mg of $Co(NO_3)_3 \cdot 6H_2O$, 291 mg of $Ni(NO_3)_2 \cdot 6H_2O$ and 88 mg of $NaH_2PO_2 \cdot H_2O$ lasting for 15 min, the deposition process was performed under -1.2 V *vs.* Ag/AgCl. The deposition time was determined according to our previous report [24]. After copious rinsing with Milli-Q water and drying at 35 ºC, the hybrid MSC consisting of $CoNiP_2O_7$@CNTs positive electrode and CNTs negative electrode

($CoNiP_2O_7$@CNTs//CNTs) was fabricated.

Preparation of KOH/PVA gel electrolyte. Typically, KOH (4 g) and PVA (4 g) were dispersed in 40 mL of Milli-Q water, and the solution was further magnetically stirred at 80 °C until ~~the mixture was~~it became transparent. The resulting gel was dropped onto the two electrodes of the MSC, and after packaging by vacuum bag (PA+PE), the hybrid MSC was totally constructed for further electrochemical measurements.

RESULTS AND DISCUSSION

Fig. 1a illustrates the schematic fabrication process of the hybrid MSC. The process comprised several stages. Firstly, a homogeneous CNTs ethanoic solution was sprayed to form the interdigitated electrodes (steps (i) and (ii)). Next, the electrodeposition of $CoNiP_2O_7$ composite (step (iii)) was performed in a typical 3-electrode configuration cell using an aqueous solution of $Co(NO_3)_3 \cdot 6H_2O$, $Ni(NO_3)_2 \cdot 6H_2O$ and $NaH_2PO_2 \cdot H_2O$. Using the CNTs electrode on the opposite position to be the negative electrode, a $CoNiP_2O_7$@CNTs//CNTs hybrid MSC was successfully fabricated. **Fig. 1b** displays the *I-V* curves of CNTs and $CoNiP_2O_7$@CNTs electrodes acquired using Semiconductor Device Parameter Analyzer (B1500A, KeySight, America) from -1 to +1 V. From the data, the resistance values could be calculated and determined as 271 and 379 Ω for CNTs and $CoNiP_2O_7$@CNTs electrodes, respectively, revealing a good conductivity. The resistance value of the pristine CNTs electrode~~s~~ is small and infers that they are suitable to operate as the negative electrode and substrate for $CoNiP_2O_7$ composite electrodeposition.

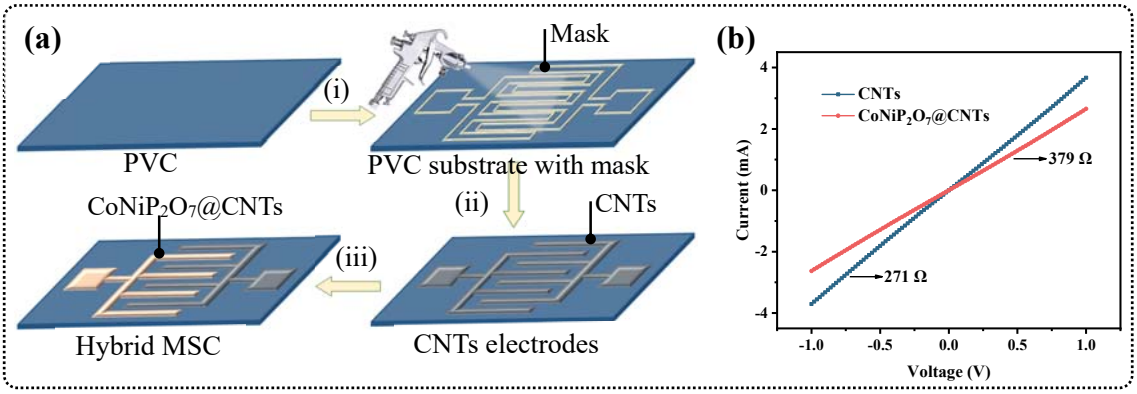

Figure 1. The schematic fabrication process of the hybrid MSC. **(i, ii)** Spraying-coating

of the interdigitated CNTs electrodes through a mask, (**iii**) Electrodeposition of $CoNiP_2O_7$ composite on one side of the CNTs electrode. (**b**) *I-V* curves of CNTs and $CoNiP_2O_7$@CNTs electrodes.

Additionally, X-ray diffraction (XRD) measurements were collected to gain insight into the composition and crystallinity of the $CoNiP_2O_7$@CNTs electrode (**Fig. S2**). The XRD pattern consisted of two weak peaks located at 29.7° and 43.2° that could be ascribed respectively to the (012) and (040) diffraction planes of cobalt nickel phosphate ($CoNiP_2O_7$) composite (JCPDS No. 48-0563) [25]. The wide peak at ~21.1° is attributed to the quartz glass substrate used in the measurement process [26].

Furthermore, X-ray photoelectron spectroscopy tests were conducted. **Fig. S3a** illustrates the survey spectrum of CNTs ~~comprised~~ comprising two main peaks due to C_{1s} and O_1 elements. The high-resolution plot of the C_{1s} in **Fig. S3b** could be fitted with C-C (sp^2) ~~bond~~ at 284.2 eV, C-C (sp^3) ~~peak~~ at 284.9 eV, C-O ~~bond~~ at 286.0 eV, and C=O ~~bond~~

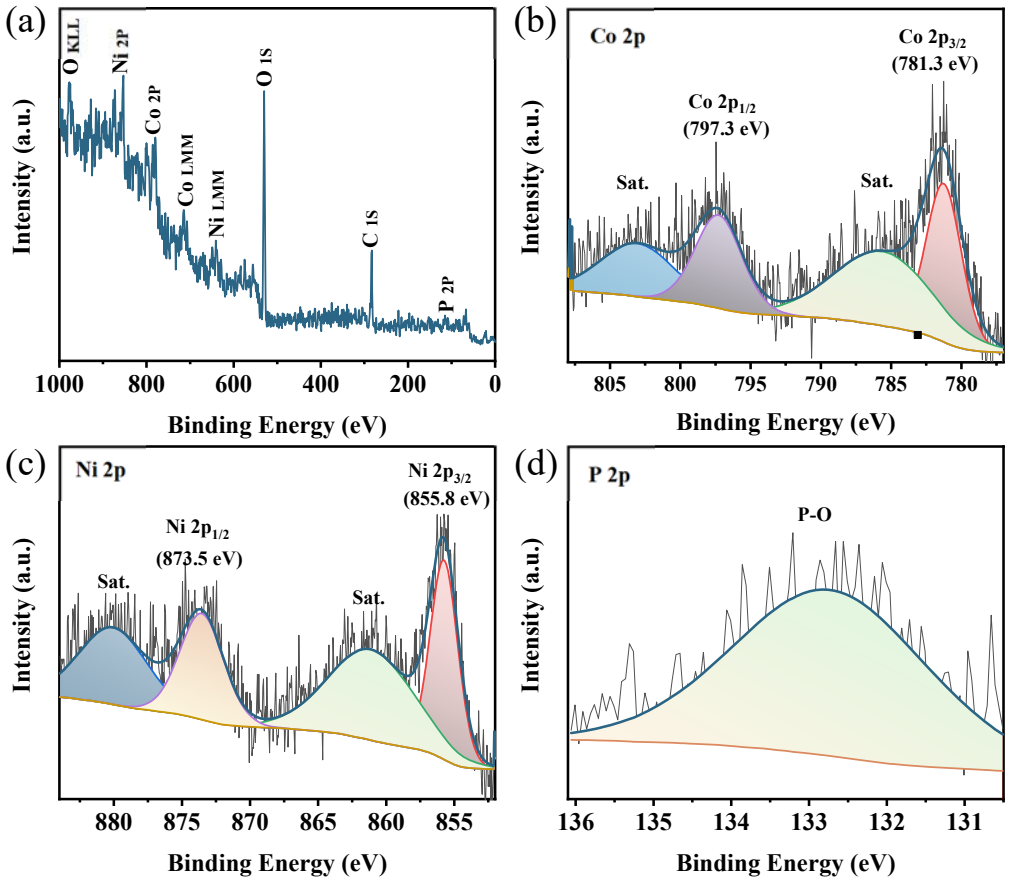

Figure 2. (**a**) XPS survey spectrum and core level spectra of the (**b**) Co_{2p}, (**c**) Ni_{2p} and (**d**) P_{2p} of the $CoNiP_2O_7$@CNTs electrode.

located at 288.6 eV ~~respectively~~ [27]. And in **Fig. S3c**, the O_{1s} peak was fitted with the typical C-O bond at 531.8 eV and C=O component at 533.1 eV ~~separately~~ [28]. Apart from C_{1s} and O_{1s} peaks, additional peaks due to Co_{2p}, Ni_{2p} and P_{2p} elements appeared in the XPS large scan of the $CoNiP_2O_7$@CNTs composite, as depicted in **Fig. 2a**. From **Fig. 2b**, it could be seen that the Co_{2p} peak could be deconvoluted into two main peaks attributed to $Co_{2p3/2}$ at 781.3 eV with satellite peak at 786.0 eV and $Co_{2p1/2}$ at 797.3 eV with satellite peak at 803.2 eV, ~~respectively,~~ which is an indication of the existence of Co in its +2 oxidation state [10]. For the Ni_{2p} element, it was also deconvoluted into $Ni_{2p3/2}$ ~~855.8 eV~~ and $Ni_{2p1/2}$ peaks at 855.8 and 873.5 eV, respectively, with two satellite components at 861.4 and 880.2 eV, revealing the occurrence of Ni (II) [29]. Meanwhile, the peak at 132.8 eV was consistent with ~~to~~ P-O bond [30], indicating the successfully preparation of $CoNiP_2O_7$ composite on CNTs.

Scanning electron microscopy (SEM) measurements were applied ~~for having an investigation on~~to investigate the surface appearance of the CNTs and $CoNiP_2O_7$ electrodes. As shown in **Fig. S4**, the 1D CNTs were intertwined with each other, forming conductive networks with numerous micro/nanopores, which are expected to be beneficial for the electrochemical performance. Furthermore, after electrodeposition process, the CNTs were decorated with $CoNiP_2O_7$ spheres; meanwhile, existence of nanopores could be still evidenced, as seen in **Fig. 3a** and **b**. **Fig. 3c** depicts the EDS elemental mapping images, which indicated the presence of Co, Ni, P, C and O elements in $CoNiP_2O_7$@CNTs and CNTs electrodes. The colors of C element turned to be darker in $CoNiP_2O_7$@CNTs electrode than that of CNTs, which is also an indication of successful deposition of $CoNiP_2O_7$ composite.

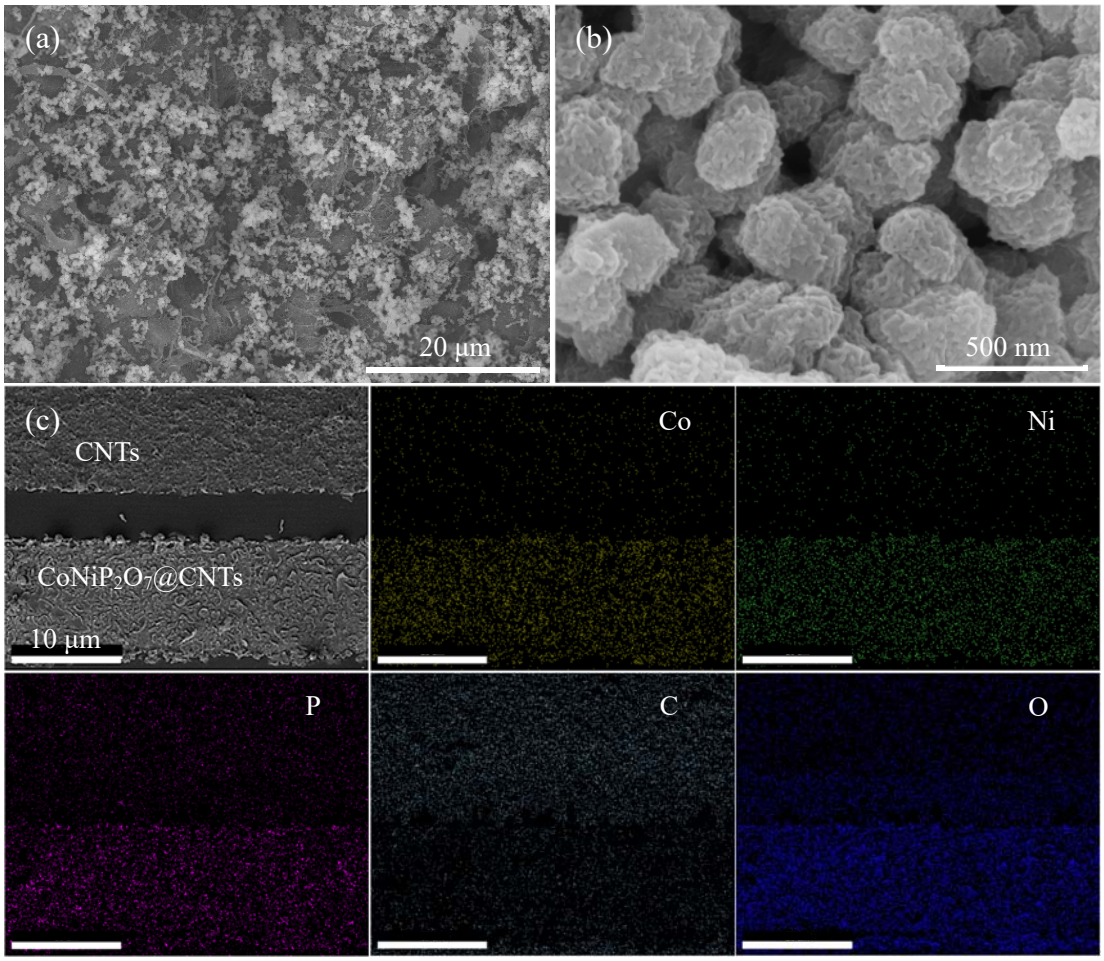

Figure 3. SEM images of the (**a**) $CoNiP_2O_7$@CNTs positive electrode. (**c**) EDS elemental mapping images of Co, Ni, P, C and O of the MSC electrodes.

Transmission electron microscopy (TEM) is another effective method to investigate the morphology of samples. **Fig. 4a** presents the TEM image of $CoNiP_2O_7$@CNTs showing that the 1D CNTs were intertwined together, ensuring the conductivity of the interdigitated electrode. The obvious dark regions on the surface were ascribed to $CoNiP_2O_7$ particles decorated onto the CNTs. **Fig.4b** displays the high-resolution TEM image of $CoNiP_2O_7$ composite**.** An ~~0.21 nm of the~~ interlayer distance of 0.21 nm assigned to the (040) plane of $CoNiP_2O_7$ could be clearly observed, which is consistent with the SAED ~~result in~~(-**Fig. 4c**) and XRD ~~result in~~(-**Fig. S2**) results. Additionally, as shown in **Fig. 4d**, the images revealed the appearance of Co, Ni, P, C and O elements with uniform distribution, in accordance with the results in **Fig. 3c**.

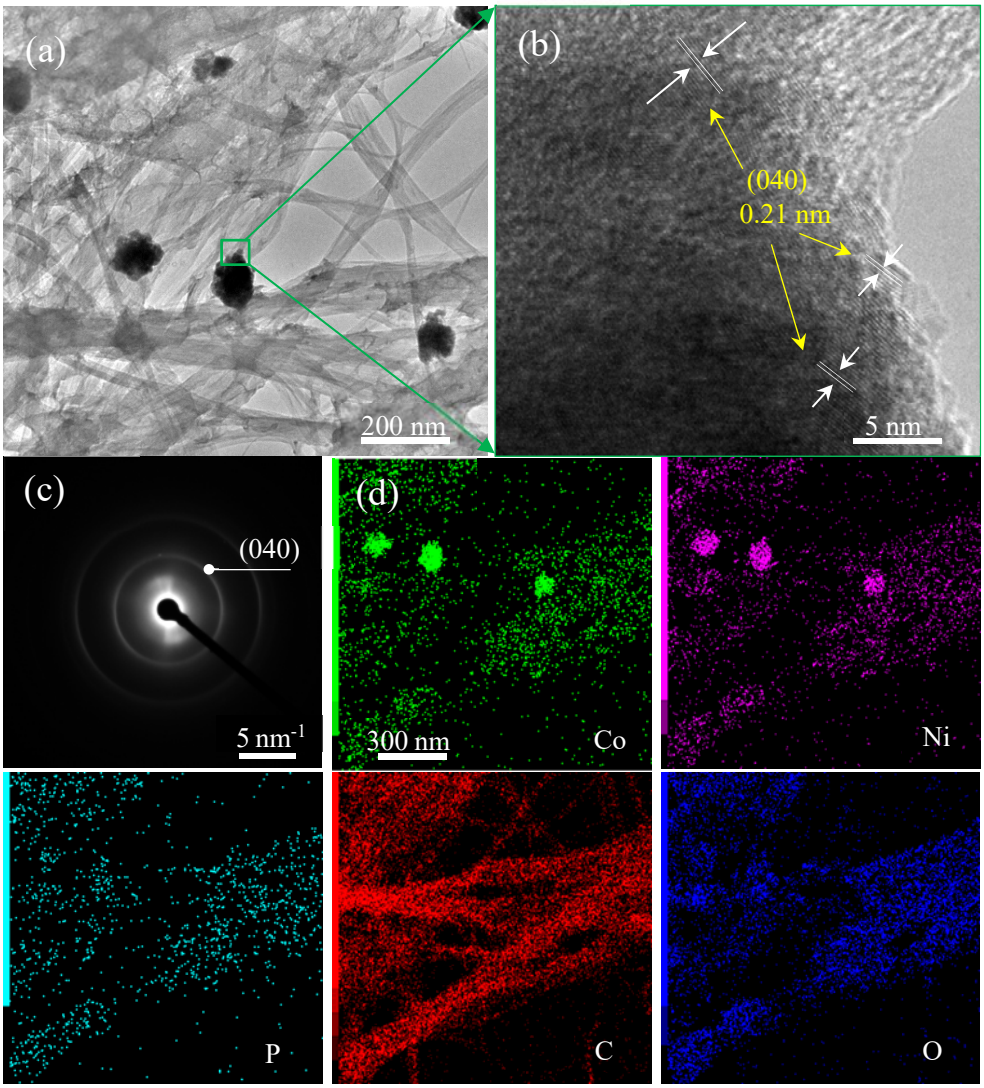

Figure 4. (**a**) TEM and (**b**) high-resolution TEM images, (**c**) SAED pattern and (**d**) the corresponding EDS elemental mapping images of Ni, Co, C and O of the of $CoNiP_2O_7$@CNTs composite.

To assess the electrochemical performance of the as-obtained $CoNiP_2O_7$@CNTs//CNTs MSC devices, CV measurements at various voltage windows were first conducted to determine the working region. As illustrated in **Fig. 5a**, the largest test voltage could range from 0 to +1.1 V. Taking the safety and damage into account, 0-1 V was set as the working voltage window, as depicted in **Fig. 5b,** which could ~~work~~ operate normally from 10 to 100 $mV \cdot s^{-1}$. To further explore charge-discharging trait of the MSC device, GCD tests were acquired from 0.08 to 0.5 $mA \cdot cm^{-2}$. The results indicated high coulombic efficiencies at different current densities, with

the smallest value (80%) was recorded at 0.08 mA cm^{-2}, as plotted and listed respectively in **Fig. 5c** and **Table S1**. Additionally, the areal capacitance values were determined ~~by~~ using **Eq. S1**. In **Fig. 5d**, the largest areal capacitance attained was 20.9 $mF \cdot cm^{-2}$ at 0.08 $mA \cdot cm^{-2}$~~,~~; ~~when measured~~this value dropped to 14.3 $mF \cdot cm^{-2}$ at 0.5 $mA \cdot cm^{-2}$~~, the value was calculated~~ as ~~14.3 mF cm^{-2}~~, indicating a favorable rate performance of 67%. Moreover, at a power density of 41.3 $\mu W \cdot cm^{-2}$, the device recorded a large energy density of 2.9 $\mu Wh \cdot cm^{-2}$, ~~which were~~as determined by **Eq. S2** and **S3** and depicted in **Fig. 5e**. It featured a better performance than previously reported MSC devices, such as electrochemically exfoliated graphene-based MSC [31], CoNiP LDHs@CNTs//CNTs MSC [32], exfoliated graphene/nano-graphene oxide ~~MSC~~ [33], Ox-SWCNT-MSC-IPL ~~MSC~~ [34], I-$Ti_3C_2T_x$ ~~MSC~~ [35], G-CNT-X ~~MSC~~ [36], MnO_2-rGO/MnO_2-CNT ~~MSC~~ [37], paper-based PEDOT:PSS-CNT/Ag ~~MSC~~ [38], GP/PANI-G/GP ~~MSC~~ [39], clay-like Ti_3C_2 MXene ~~based MSC device~~ [40], MnO_2/OLC ~~MSC~~ [41], and TiO_2-based MSCs [42], ~~as the values shown in~~ **Table 1**.

Additionally, the EIS test of the $CoNiP_2O_7$@CNTs//CNTs MSC device was conducted and illustrated in **Fig. S5**~~,~~. ~~the~~ The R_s and R_{ct} were determined as 160.3 and 103.3 $ohm \cdot cm^{-2}$; these small values are a good indication of the high electrochemical performance. The stability and reversibility are critical parameters for practical application of MSC devices. The ~~measurement~~ stability of $CoNiP_2O_7$@CNTs//CNTs was ~~carried out~~assessed by repeating the GCD test for 5000 cycles. The data in **Fig. 5f** revealed that the areal capacitance retained ~82% of the original value after 5000 cycling tests, ~~indicating~~ implying good stability and reversibility of the as-assembled MSC device.

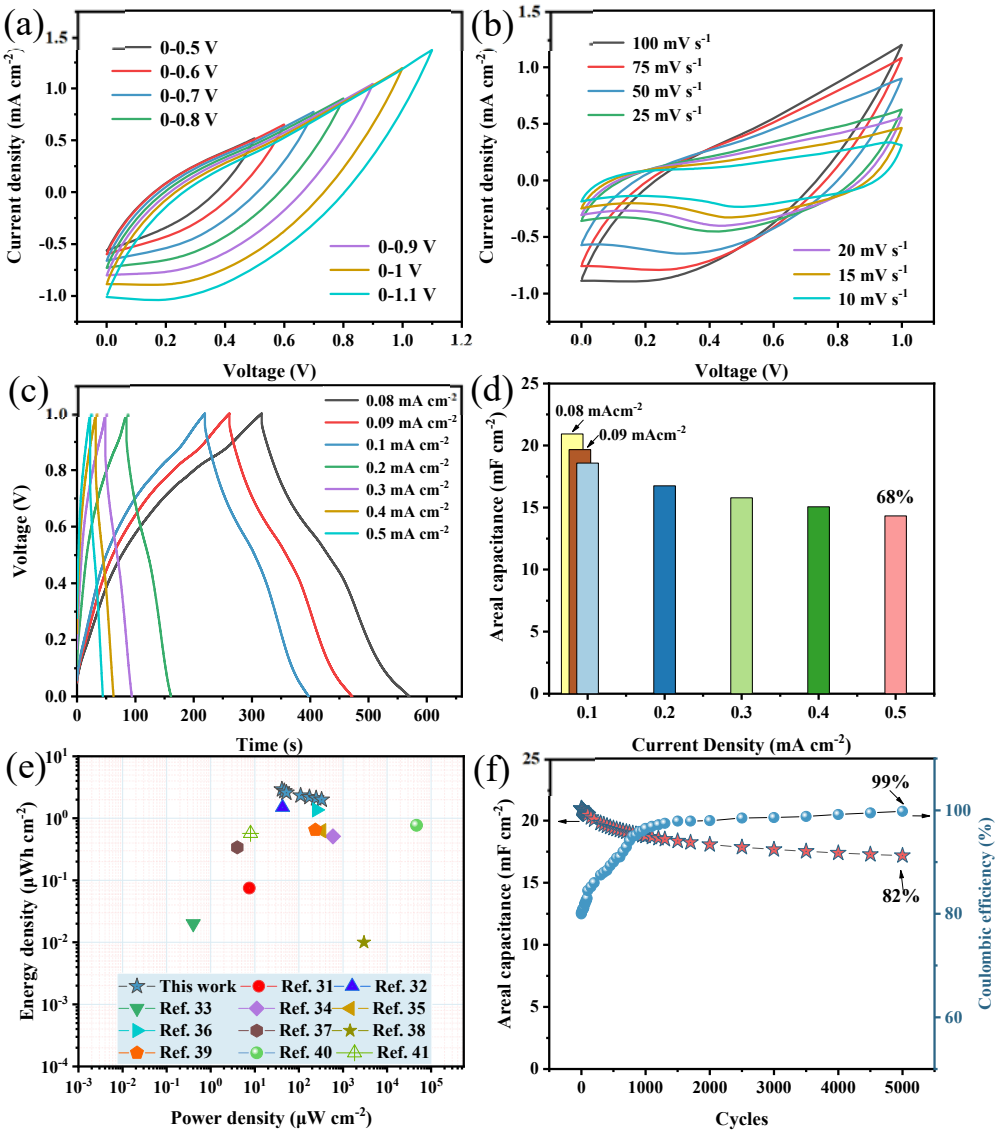

Figure 5. Electrochemical performance of the hybrid $CoNiP_2O_7$@CNTs//CNTs MSC. CV curves at (**a**) various working windows and (**b**) different scan rates, (**c**) GCD plots, (**d**) areal capacitance, (**e**) Ragone profiles, and (**f**) stability test at 0.08 mA·cm^{-2}.

Table 1 Comparison of different MSC devices.

MSC devices	Energy density ($\mu Wh \cdot cm^{-2}$)	Power density ($\mu W \cdot cm^{-2}$)	References
Exfoliated graphene ~~-based MSC~~	0.075	7.5	[31]
CoNiP LDHs@CNTs//CNTs ~~MSC~~	1.5	42.5	[32]
Exfoliated graphene /nano-graphene oxide ~~MSC~~	0.02	0.4	[33]
Ox-SWCNT-MSC-IPL ~~MSC~~	0.51	590	[34]
I-$Ti_3C_2T_x$ ~~MSC~~	0.63	330	[35]
G-CNT-X ~~MSC~~	1.36	250	[36]
MnO_2-rGO/MnO_2-CNT ~~MSC~~	0.34	4	[37]
~~paper~~Paper-based PEDOT:PSS-CNT/Ag ~~MSC~~	0.01	3000	[38]
GP/PANI-G/GP ~~MSC~~	0.65	236	[39]
~~clay~~Clay-like Ti_3C_2 MXene ~~-based MSC~~	0.77	46600	[40]
MnO_2/OLC ~~MSC~~	0.57	8	[41]
TiO_2 ~~-based MSC~~	0.09	0.125 $A \cdot cm^{-3}$	[42]
$CoNiP_2O_7$@CNTs//CNTs ~~MSC~~	**2.9**	**41.3**	**This work**

It was necessary to conduct experiment to verify the as-proposed $CoNiP_2O_7$@CNTs//CNTs MSC device~~s~~' practical application capacity as energy storage device. As featured in **Fig. 6a**, the working voltage of two $CoNiP_2O_7$@CNTs//CNTs MSC devices in series could reach 2 V, which could be applied as energy supply for ~~the~~ a LED indicator (1.8-2 V). At the same time, to utilize natural resources in daily life, as depicted in **Fig. 6b**, an energy system, ~~was built~~ composed of solar cells (energy collection and conversion) and MSC devices (energy storage), was built. The corresponding equivalent circuit is displayed in **Fig. 6c**. At first, the solar cells were under operation state to supply power to the LED indicator and charge the MSC devices simultaneously. When the voltage between MSC devices reached 2 V, the switch was turned off suddenly that means there was no sunshine, and the LED indicator was still on for ~50 s, as the energy for its operation was supplied by

the MSC devices~~, which could be lasted ~ 50 s~~ (**Fig. 6d**). The overall energy conversion efficiency was calculated ~~by~~ using **Eq. S4** [43] and determined as ~3.1%. All the results above ~~were~~ are a good indication of the application potential of the ~~proposed~~ developed $CoNiP_2O_7$@CNTs//CNTs MSC~~s~~ as an energy storage device~~s~~.

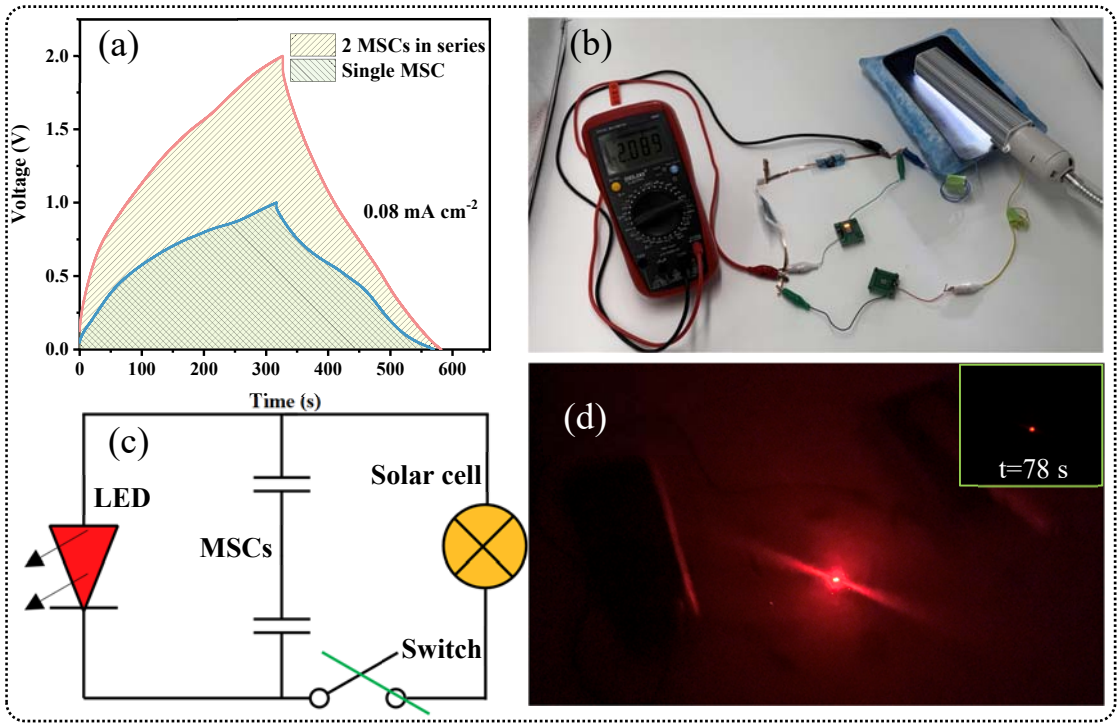

Figure 6. (**a**) GCD plots at 0.08 mA cm^{-2}. (**b**) photographs and (**c**) equivalent circuit of the sunlight-powered energy storage system. (**d**) Work state of the sunlight-powered energy storage system.

CONCLUSION

In summary, a hybrid MSC device~~s~~ ~~were~~ was assembled by combining $CoNiP_2O_7$@CNTs positive and CNTs negative electrodes. Firstly, the interdigitated CNTs electrodes were prepared by spraying-coating method. Moreover, the battery-like $CoNiP_2O_7$ composite was electrodeposited on CNT electrodes, forming $CoNiP_2O_7$@CNTs positive electrode. The largest areal capacitance of $CoNiP_2O_7$@CNTs//CNTs MSC was determined as 20.9 mF·cm^{-2} at 0.08 mA·cm^{-2}. ~~It~~ The device exhibited a largest energy density of 2.9 μWh·cm^{-2} at a power density of 41.3 μW·cm^{-2}. Furthermore, $CoNiP_2O_7$@CNTs//CNTs MSC~~it~~ was utilized for operating a red LED after storing energy from solar cells successfully in the natural

energy collection-conversion-storage-utilization system. The proposed MSC energy storage devices exhibits promising application potential in next-generation wearable and portable electronic devices.

ACKNOWLEDGEMENTS

This work is supported by the Shaanxi 2023 Natural Science Basic Research Plan (grant number 2023-JC-QN-0489), the National Key Research & Development (R&D) Program of China (grant number 2022YFB3205400), the National Natural Science Foundation of China (grant numbers 52175548, U1909221), and the Chongqing Natural Science Basic Research Project (cstc2021jcyj-msxmX0801). R. B. thanks the ANR for financial support of the project "SIREVIVAL" of the LEAP-RE programme that received funding from the European Union's Horizon 2020 Research and Innovation Program under Grant Agreement 963530.

REFERENCES

[1] X. Li, Y. Ma, Y. Yue, G. Li, C. Zhang, M. Cao, Y. Xiong, J. Zou, Y. Zhou, Y. Gao, A flexible Zn-ion hybrid micro-supercapacitor based on MXene anode and V_2O_5 cathode with high capacitance, Chem. Eng. J. 428 (2022) 130965.

[2] Y. Lei, W. Zhao, Y. Zhu, U. Buttner, X. Dong, H.N. Alshareef, Three-dimensional $Ti_3C_2T_x$ MXene-prussian blue hybrid microsupercapacitors by water lift-off lithography, ACS Nano 16 (2022) 1974-1985.

[3] Y. Chen, M. Guo, L. Xu, Y. Cai, X. Tian, X. Liao, Z. Wang, J. Meng, X. Hong, L. Mai, In-situ selective surface engineering of graphene micro-supercapacitor chips, Nano Res. 15 (2021) 1492-1499.

[4] P. Huang, C. Lethien, S. Pinaud, K. Brousse, R. Laloo, V. Turq, M. Respaud, A. Demortiere, B. Daffos, P.L. Taberna, B. Chaudret, Y. Gogotsi, P. Simon, On-chip and freestanding elastic carbon films for micro-supercapacitors, Science 351 (2016) 691-695.

[5] Y. Yuan, L. Jiang, X. Li, P. Zuo, C. Xu, M. Tian, X. Zhang, S. Wang, B. Lu, C. Shao, B. Zhao, J. Zhang, L. Qu, T. Cui, Laser photonic-reduction stamping for graphene-

based micro-supercapacitors ultrafast fabrication, Nat. Commun. 11 (2020) 6185.
[6] Y. Wang, Y. Zhao, Y. Han, X. Li, C. Dai, X. Zhang, X. Jin, C. Shao, B. Lu, C. Wang, H. Cheng, F. Liu, L. Qu, Fixture-free omnidirectional prestretching fabrication and integration of crumpled in-plane micro-supercapacitors, Sci. Adv. 8 (2022) eabn8338.
[7] C. Zhang, Z. Peng, C. Huang, B. Zhang, C. Xing, H. Chen, H. Cheng, J. Wang, S. Tang, High-energy all-in-one stretchable micro-supercapacitor arrays based on 3D laser-induced graphene foams decorated with mesoporous ZnP nanosheets for self-powered stretchable systems, Nano Energy 81 (2021) 105609.
[8] G. Shi, Y. Zhu, M. Batmunkh, M. Ingram, Y. Huang, Z. Chen, Y. Wei, L. Zhong, X. Peng, Y.L. Zhong, Cytomembrane-Inspired MXene ink with amphiphilic surfactant for 3D printed microsupercapacitors, ACS Nano 16 (2022) 14723-14736.
[9] G. Shao, R. Yu, X. Zhang, X. Chen, F. He, X. Zhao, N. Chen, M. Ye, X.Y. Liu, Making stretchable hybrid supercapacitors by knitting non-stretchable metal fibers, Adv. Funct. Mater. 30 (2020) 2003153.
[10] W. Qiao, B. Jin, W. Xie, M. Shao, M. Wei, Hierarchical CoNi-LDH nanosheet array with hydrogen vacancy for high-performance aqueous battery cathode, J. Energy Chem. 69 (2022) 9-15.
[11] Z. Shi, G. Sun, R. Yuan, W. Chen, Z. Wang, L. Zhang, K. Zhan, M. Zhu, J. Yang, B. Zhao, Scalable fabrication of $NiCo_2O_4$/reduced graphene oxide composites by ultrasonic spray as binder-free electrodes for supercapacitors with ultralong lifetime, J. Mater. Sci. Technol. 99 (2022) 260-269.
[12] G. Sun, H. Ren, Z. Shi, L. Zhang, Z. Wang, K. Zhan, Y. Yan, J. Yang, B. Zhao, V_2O_5/vertically-aligned carbon nanotubes as negative electrode for asymmetric supercapacitor in neutral aqueous electrolyte, J. Colloid Interf. Sci. 588 (2021) 847-856.
[13] Y.F. Wu, Y.C. Hsiao, C.H. Liao, C.S. Hsu, S. Yougbare, L.Y. Lin, Novel design of Sulfur-doped nickel cobalt layered double hydroxide and polypyrrole nanotube composites from zeolitic imidazolate Framework-67 as efficient active material of battery supercapacitor hybrids, J. Colloid Interf. Sci. 628 (2022) 540-552.
[14] P.Y. Lee, T.M. Cheng, S. Yougbare, L.Y. Lin, Design of novel self-assembled MXene and ZIF67 derivative composites as efficient electroactive material of energy

storage device, J. Colloid Interf. Sci. 618 (2022) 219-228.

[15] T.Y. Chen, T.R. Kuo, S. Yougbare, L.Y. Lin, C.Y. Xiao, Novel direct growth of ZIF-67 derived Co_3O_4 and N-doped carbon composites on carbon cloth as supercapacitor electrodes, J. Colloid Interf. Sci. 608 (2022) 493-503.

[16] P.Y. Lee, L.Y. Lin, Developing zeolitic imidazolate frameworks 67-derived fluorides using 2-methylimidazole and ammonia fluoride for energy storage and electrocatalysis, Energy 239 (2022) 122129.

[17] J. Huang, Y. Xiao, Z. Peng, Y. Xu, L. Li, L. Tan, K. Yuan, Y. Chen, Co_3O_4 supraparticle-based bubble nanofiber and bubble nanosheet with remarkable electrochemical performance, Adv. Sci. 6 (2019) 1900107.

[18] J. Li, S. Luo, B. Zhang, J. Lu, W. Liu, Q. Zeng, J. Wan, X. Han, C. Hu, High-performance asymmetric $Mn(OH)_2$//Fe_2O_3 supercapacitor achieved by enhancing and matching respective properties of cathode and anode materials, Nano Energy 79 (2021) 105410.

[19] M. Li, A. Addad, Y. Zhang, A. Barras, P. Roussel, M.A. Amin, S. Szunerits, R. Boukherroub, Flower-like Nitrogen-co-doped MoS_2@RGO composites with excellent stability for supercapacitors, ChemElectroChem 8 (2021) 2903-2911.

[20] L. Wan, C. He, D. Chen, J. Liu, Y. Zhang, C. Du, M. Xie, J. Chen, In situ grown NiFeP@$NiCo_2S_4$ nanosheet arrays on carbon cloth for asymmetric supercapacitors, Chem. Eng. J. 399 (2020) 125778.

[21] J. Huang, Y. Xiong, Z. Peng, L. Chen, L. Wang, Y. Xu, L. Tan, K. Yuan, Y. Chen, A general electrodeposition strategy for fabricating ultrathin nickel cobalt phosphate nanosheets with ultrahigh capacity and rate performance, ACS Nano 14 (2020) 14201-14211.

[22] Z. Xiao, Y. Bao, Z. Li, X. Huai, M. Wang, P. Liu, L. Wang, Construction of hollow cobalt–nickel phosphate nanocages through a controllable etching strategy for high supercapacitor performances, ACS Appl. Energy Mater. 2 (2019) 1086-1092.

[23] H.C. Chen, S. Jiang, B. Xu, C. Huang, Y. Hu, Y. Qin, M. He, H. Cao, Sea-urchin-like nickel-cobalt phosphide/phosphate composites as advanced battery materials for hybrid supercapacitors, J. Mater. Chem. A 7 (2019) 6241-6249.

[24] M. Li, Y. Luo, C. Jia, Q. Zhang, G. Luo, L. Zhao, R. Boukherroub, Z. Jiang, Facile synthesis of bimetal nickel cobalt phosphate nanostructures for high-performance hybrid supercapacitors, J. Alloy. Compd. 893 (2021) 162340.

[25] F.F. Li, Z.H. He, J.F. Gao, L.B. Kong, The investigations of pyrophosphate $CoNiP_2O_7$ produced by hydrothermal process: a high-performance anode electrode material for Li-ion hybrid capacitor, Ionics 26 (2020) 2989-3001.

[26] A.I. Nepomnyashchikh, A.A. Shalaev, T.Y. Sizova, A.S. Paklin, A.N. Sapozhnikov, L.A. Pavlova, Onset Temperatures and kinetics of quartz glass crystallization, Crystallog. Rep. 63 (2018) 290-294.

[27] L. Feng, Y. Zuo, X. He, X. Hou, Q. Fu, H. Li, Q. Song, Development of light cellular carbon nanotube@graphene/carbon nanocomposites with effective mechanical and EMI shielding performance, Carbon 168 (2020) 719-731.

[28] L. Song, X. Cao, L. Li, Q. Wang, H. Ye, L. Gu, C. Mao, J. Song, S. Zhang, H. Niu, General method for large-area films of carbon nanomaterials and application of a self-assembled carbon nanotube film as a high-performance electrode material for an all-solid-state supercapacitor, Adv. Funct. Mater. 27 (2017) 1700474.

[29] L. Zhang, P. Cai, Z. Wei, T. Liu, J. Yu, A.A. Al-Ghamdi, S. Wageh, Synthesis of reduced graphene oxide supported nickel-cobalt-layered double hydroxide nanosheets for supercapacitors, J. Colloid Interf. Sci. 588 (2021) 637-645.

[30] W. Mai, Q. Cui, Z. Zhang, K. Zhang, G. Li, L. Tian, W. Hu, CoMoP/NiFe-layered double-hydroxide hierarchical nanosheet arrays standing on ni foam for efficient overall water splitting, ACS Appl. Energy Mater. 3 (2020) 8075-8085.

[31] J. Li, S. Sollami Delekta, P. Zhang, S. Yang, M.R. Lohe, X. Zhuang, X. Feng, M. Ostling, Scalable fabrication and integration of graphene microsupercapacitors through full inkjet printing, ACS Nano 11 (2017) 8249-8256.

[32] M. Li, C. Jia, D. Zhang, Y. Luo, L. Wang, P. Yang, G. Luo, L. Zhao, R. Boukherroub, Z. Jiang, Facile assembly of hybrid micro-supercapacitors for a sunlight-powered energy storage system, ACS Appl. Mater. Interfaces 14 (2022) 47595-47604.

[33] S. Sollami Delekta, K.H. Adolfsson, N. Benyahia Erdal, M. Hakkarainen, M. Ostling, J. Li, Fully inkjet printed ultrathin microsupercapacitors based on graphene

electrodes and a nano-graphene oxide electrolyte, Nanoscale 11 (2019) 10172-10177.
[34] A. Jo, S.I. Chung, P.K. Kim, J.W. Lee, H.J. Lee, H.J. Yang, T.G. Ha, J. Kim, Y.J. Lee, H.J. Jeong, S.H. Seo, S.Y. Jeong, G.W. Lee, K.J. Baeg, J.T. Han, J.H. Park, All-printed paper-based micro-supercapacitors using water-based additive-free oxidized single-walled carbon nanotube pastes, ACS Appl. Energy Mater. 4 (2021) 13666-13675.
[35] C.J. Zhang, M.P. Kremer, A. Seral-Ascaso, S.H. Park, N. McEvoy, B. Anasori, Y. Gogotsi, V. Nicolosi, Stamping of flexible, coplanar micro-supercapacitors using mxene inks, Adv. Funct. Mater. 28 (2018) 1705506.
[36] Y. Wang, Y. Zhang, G. Wang, X. Shi, Y. Qiao, J. Liu, H. Liu, A. Ganesh, L. Li, Direct graphene-carbon nanotube composite ink writing all‐solid‐state flexible microsupercapacitors with high areal energy density, Adv. Funct. Mater. 30 (2020) 1907284.
[37] B.D. Boruah, A. Maji, A. Misra, Flexible array of microsupercapacitor for additive energy storage performance over a large area, ACS Appl. Mater. Interfaces 10 (2018) 15864-15872.
[38] W. Liu, C. Lu, H. Li, R.Y. Tay, L. Sun, X. Wang, W.L. Chow, X. Wang, B.K. Tay, Z. Chen, J. Yan, K. Feng, G. Lui, R. Tjandra, L. Rasenthiram, G. Chiu, A. Yu, Paper-based all-solid-state flexible micro-supercapacitors with ultra-high rate and rapid frequency response capabilities, J. Mater. Chem. A 4 (2016) 3754-3764.
[39] X. Shi, Z.S. Wu, J. Qin, S. Zheng, S. Wang, F. Zhou, C. Sun, X. Bao, Graphene-based linear tandem micro-supercapacitors with metal-free current collectors and high-voltage output, Adv. Mater. 29 (2017) 1703034.
[40] N. Kurra, B. Ahmed, Y. Gogotsi, H.N. Alshareef, MXene-on-paper coplanar microsupercapacitors, Adv. Energy Mater. 6 (2016) 1601372.
[41] Y. Wang, Y. Shi, C.X. Zhao, J.I. Wong, X.W. Sun, H.Y. Yang, Printed all-solid flexible microsupercapacitors: towards the general route for high energy storage devices, Nanotechnology 25 (2014) 094010.
[42] M. Salari, S.H. Aboutalebi, I. Ekladious, R. Jalili, K. Konstantinov, H.K. Liu, M.W. Grinstaff, Tubular TiO_2 nanostructures: toward safer microsupercapacitors, Adv. Mater. Technol. 3 (2018) 1700194.

[43] Y. Yuan, Y. Lu, B.E. Jia, H. Tang, L. Chen, Y.J. Zeng, Y. Hou, Q. Zhang, Q. He, L. Jiao, J. Leng, Z. Ye, J. Lu, Integrated system of solar cells with hierarchical $NiCo_2O_4$ battery-supercapacitor hybrid devices for self-driving light-emitting diodes, Nano-Micro Lett. 11 (2019) 42.